Beyond simple self-healing: How anisotropic nanogels adapt their shape to their environment

Cite as: J. Chem. Phys. 157, 194901 (2022); doi: 10.1063/5.0119527 Submitted: 9 August 2022 • Accepted: 24 October 2022 •







Published Online: 15 November 2022

Anne C. Nickel,¹ Alan R. Denton,² D Judith E. Houston,³ Ralf Schweins,⁴ Tomàs S. Plivelic,⁵ Walter Richtering,¹ D and Andrea Scotti^{1,a)} D

AFFILIATIONS

- ¹Institute of Physical Chemistry, RWTH Aachen University, 52056 Aachen, Germany
- ² Department of Physics, North Dakota State University, Fargo, North Dakota 58108-6050, USA
- ³European Spallation Source ERIC, Box 176, SE-221 00 Lund, Sweden
- ⁴Institut Laue-Langevin ILL DS/LSS, 71 Avenue des Martyrs, F-38000 Grenoble, France
- ⁵MAX IV Laboratory, Lund University, P.O. Box 118, 22100 Lund, Sweden

Note: This paper is part of the JCP Special Topic on Colloidal Gels.

a) Author to whom correspondence should be addressed: scotti@pc.rwth-aachen.de

ABSTRACT

The response of soft colloids to crowding depends sensitively on the particles' compressibility. Nanogel suspensions provide model systems that are often studied to better understand the properties of soft materials and complex fluids from the formation of colloidal crystals to the flow of viruses, blood, or platelet cells in the body. Large spherical nanogels, when embedded in a matrix of smaller nanogels, have the unique ability to spontaneously deswell to match their size to that of the nanogel composing the matrix. In contrast to hard colloids, this self-healing mechanism allows for crystal formation without giving rise to point defects or dislocations. Here, we show that anisotropic ellipsoidal nanogels adapt both their size and their shape depending on the nature of the particles composing the matrix in which they are embedded. Using small-angle neutron scattering with contrast variation, we show that ellipsoidal nanogels become spherical when embedded in a matrix of spherical nanogels. In contrast, the anisotropy of the ellipsoid is enhanced when they are embedded in a matrix of anisotropic nanogels. Our experimental data are supported by Monte Carlo simulations that reproduce the trend of decreasing aspect ratio of ellipsoidal nanogels with increasing crowding by a matrix of spherical nanogels.

Published under an exclusive license by AIP Publishing. https://doi.org/10.1063/5.0119527

I. INTRODUCTION

The main characteristic of a soft object is its capability to adapt its shape and volume to crowding. This response can be achieved by either changing the volume at a constant shape or changing the shape at a constant volume. The compressibility of the soft building blocks composing soft materials has a great impact on the macroscopic properties of the material itself. For instance, the deformation of platelet cells is fundamental for the successful clotting of wounds. Furthermore, the compressibility of the soft building blocks, e.g., the deformation of colloidal particles composing a paint or a cosmetic cream, has a strong impact on the adhesion of the material itself on the surface where it is spread. The spread is spread.

Nanogels are a model system for compressible soft spheres, largely used both to understand fundamental principles of phase

transitions⁶⁻¹¹ and flow properties of complex fluids.¹²⁻¹⁵ Furthermore, nanogel suspensions are used to develop new soft materials, such as synthetic platelets¹⁶ or thermo-responsive supports for 3D growth of cells.^{17,18} These particles are crosslinked polymeric networks that show a behavior in between that of hard incompressible colloids and flexible polymer coils.¹⁹ Nanogels are swollen in a good solvent and, depending on changes in external stimuli, such as temperature or pH, can undergo a volume phase transition.²⁰ The compressibility of nanogels largely affects both the phase behavior and the flow properties of the suspension.^{10,11,13,14,21,22} The use of super-resolved fluorescence microscopy has directly shown how isotropic deswelling and faceting play a role once nanogels are in crowded environments.⁹ This information has then been used to rationalize the elastic and dissipative response of nanogel suspensions under flow.²¹ As mentioned, the capability of nanogels to

adapt their size and shape in crowded environments has a strong impact on their equilibrium phase behavior. 7,11,23,24 One of the most studied properties of nanogels in crowded environments is their selfhealing behavior:^{25,26} When a few large nanogels are mixed with a majority of smaller nanogels, the bigger particles spontaneously decrease their size to fit into the lattice formed by the smaller particles without generating point defects. 25,26 This mechanism has been explained in terms of the increase in osmotic pressure due to the counterion clouds surrounding the nanogels.²⁷ Once these clouds have percolated the available volume outside nanogels, the counterions bound at the periphery of the nanogels can be considered as effective degrees of freedom of the suspensions and a jump in the osmotic pressure of the solution is measured. As soon as the solution osmotic pressure is larger than the bulk modulus of the larger nanogels, they deswell first. 7,27,28 As a consequence, point defects or dislocations are eliminated and solutions of soft spheres can crystallize even when the nanogel size distribution is highly polydisperse

The aforementioned studies focused only on spherical soft particles. For incompressible colloids, the particles' anisotropy has been shown to change the self-assembly in the presence of external fields^{29,30} and the maximum attainable packing fraction.^{31,32} One could expect that softness affects the suspension phase behavior and macroscopic properties of the suspension as it does for spherical colloids. So far, there are only few experimental studies to support this hypothesis due to the severe challenges related to synthesizing anisotropic soft particles. 33,34 In terms of applications, the interactions with cells are influenced by shape anisotropy of nanoparticles. For instance, it is known that the internalization is strongly shapedependent.35-41 Moreover, in this case, there are only a few studies on the interplay between softness and anisotropy for colloids in biological environments. 40-43 Recent advances in the synthetic protocols lead to the realization of anisotropic micro- and nanogels with different internal structures, such as core-shell and hollow. §4,44,45 In a previous study, we used a multi-step synthesis that, starting from a sacrificial ellipsoidal core on which a polymeric shell is grown, leads to the production of soft anisotropic nanogels.44

Here, we combine small-angle neutron scattering (SANS) with contrast variation and small-angle x-ray scattering (SAXS) to study the response of ellipsoidal soft nanogels to crowding. The ellipsoidal nanogels are hollow since they are obtained from the dissolution of a sacrificial ellipsoidal core. 44

To date, to obtain anisotropic nanogels, a multi-step synthesis is required, where the polymeric shell grows onto a sacrificial ellipsoidal core. Therefore, the hollow nature of the ellipsoidal nanogels is inevitable in this study. These ellipsoidal nanogels are embedded in a matrix of spherical nanogels synthesized using a comparable amount of crosslinker agents. In this environment, the ellipsoidal particles become more and more spherical upon increasing the concentration of the spherical nanogels. In contrast, if the same ellipsoidal nanogels are embedded in a matrix of identical ellipsoidal nanogels, the effect of crowding is to enhance the particle anisotropy. The shape of the nanogel in concentrated suspension is directly measured using SANS with contrast variation. Our results are supported by Monte Carlo simulations and rationalized by considering the work needed to deswell and deform the ellipsoidal nanogels. The picture that emerges is that these anisotropic soft particles extend the mechanism of self-healing and can selectively change both their size and shape (i.e., remain ellipsoidal or become spherical), depending on the shape of the surrounding particles.

II. EXPERIMENTAL SECTION

A. Materials

All materials were used as purchased. Ammonia solution (28%-30%), potassium peroxydisulfate (KPS), tetra-ethyl orthosilicate (TEOS), sodium dihydrogen phosphate monohydrate (NaH₂PO₄), and concentrated HCl were obtained from Merck. Absolute ethanol and NaOH were obtained from VWR chemicals. Heavy water (D₂O, 99.9%) was purchased from Deutero GmbH. The used deuterated N-isopropylacrylamide (D7-NIPAM) was purchased from Polymer Source, and iron(III) perchlorate hydrate [(Fe(ClO₄)₃) × H₂O] was from Aldrich. The crosslinker N,N'methylene-bisacrylamide (BIS), urea, polyvinylpyrrolidone (PVP), and tetramethylammonium hydroxide (TMAH) (25 wt. %) were bought at Sigma-Aldrich, the co-monomer N,N'-bis(acryloyl) cystamine (BAC) was purchased from Alfa Aesar, and the monomer NIPAM was purchased at Acro organics. 3-(trimethyloxysilyl) propylmethacrylate (MPS) was obtained from PanReac AppliChem. The water used for synthesis and purification was doubled-distilled Milli-Q water.

B. Synthesis of anisotropic hollow nanogel shells

A mixture of 516.1 mg NIPAM, 40.7 mg BIS, 14.7 mg of cores, and the 3 ml core solution was dispersed in 280 ml of filtered, double-distilled Milli-Q water within a three-neck flask, equipped with a reflux cooler and an overhead stirrer. All the details regarding the synthesis of the cores are reported in Appendix B. The solution was stirred at 200 R/min, degassed with nitrogen for 1 h, and simultaneously heated to 60 °C with an oil bath. After 45 min, the temperature of the oil bath was adjusted to 80 °C, and when the oil bath reached 80 °C, a solution of 40.8 mg KPS in 10 ml of filtered, double-distilled water was added dropwise to start the reaction. This initiator solution was previously degassed directly in a 20 ml syringe. 4 h after the reaction was started, the solution was cooled to room temperature and the nitrogen flow was stopped to end the reaction. The anisotropic core-shell nanogels were cleaned with threefold centrifugation and redispersing in fresh filtered, double-distilled Milli-O water.

For the shell synthesis of the anisotropic deuterated nanogels, 1.1998 g D7-NIPAM ($C_6D_7H_4NO$), 79.5 mg BIS, 5 ml core solution, and 80.6 mg KPS were used.

Both the core–shell nanogels were then treated with HCl solution to etch the hematite spindles and then with sodium hydroxide solution to remove the silica. The concentrations of these samples is expressed in weight fraction since, to the best of our knowledge, there is not a simple relation between the weight fraction and the generalized packing fraction for ellipsoidal colloids.

C. Synthesis of deuterated matrix nanogels

The same batch of spherical deuterated nanogels used in Scotti *et al.*⁴⁶ was used in this study. For the synthesis, 1.4280 g D7-NIPAM, 96.4 mg BIS, and 19.2 mg sodium dodecyl sulfate (SDS) were dissolved in 80 ml filtered double-distilled water. The suspension was degassed by purging with nitrogen under stirring at

200 rpm and 60 °C. As an initiator, a solution of 35.2 mg KPS in 5 ml water was degassed. The precipitation polymerization was initiated by transferring the initiator solution rapidly to the monomer solution. The reaction was left to proceed for 4 h. Ultra-centrifugation and lyophilization were used for purification and storage.

For spherical nanogels, it is possible to establish a linear relation between the weight fraction and the generalized packing fraction of nanogels in suspension. Such a relation holds for regular, ultra-soft, and hollow spherical nanogels. 11,46,47 In our previous study, a value of 29.4 \pm 0.6 was obtained for this conversion constant by fitting the data of the relative viscosity of diluted solution of these particles with the Einstein-Batchelor equation.⁴⁶

D. Small-angle neutron scattering

The SANS experiments were performed on the D11 instrument at the Institut Laue-Langevin (ILL, Grenoble, France). The q-range of interest was covered using three configurations: Sample-to-detector distance, $d_{SD} = 34$ m with neutron wavelength λ = 0.6 nm, d_{SD} = 8 m with λ = 0.6 nm, and d_{SD} = 2 m with $\lambda = 0.6$ nm for the anisotropic nanogels in a matrix of spherical nanogels and in a matrix of anisotropic nanogels. The instrument is equipped with a ³He detector, and the wavelength resolution was $\Delta \lambda/\lambda = 9\%$. The form factor of the hydrogenated anisotropic nanogels and their mixtures with the spherical deuterated nanogels was measured in a mixture of 90 wt. $^{-}$ D2O and 10 wt. $^{\times}$ H2O to contrast-match the spherical nanogels.46 The mixtures of hydrogenated anisotropic nanogels with deuterated anisotropic nanogels were measured in a mixture of 83 wt. % D2O and 17 wt. % H2O to contrast-match the deuterated anisotropic nanogels. 11,47

E. Small-angle x-ray scattering

Synchrotron SAXS experiments were performed at the CoSAXS beamline at the 3 GeV ring of the MAX IV Laboratory in Lund, Sweden.⁴⁹ CoSAXS was operated with a sample-to-detector distance of 6.9 m with x-ray beam energy E = 12.4 keV giving a q-range of 0.014-1.40 nm⁻¹. Data were collected using a Eiger2 4M SAXS detector with pixel size of 75 \times 75 μ m². The 2D images were converted to 1D profiles using the data reduction software DAWN.⁵⁰

F. Flory-Hertz model of nanogels

To interpret the experimental measurements, we performed Monte Carlo simulations of a coarse-grained model of an ellipsoidal nanogel in a concentrated solution of spherical nanogels. We denote the dry and swollen radii of the spherical nanogels by a_0 and a, respectively. Consistent with the experimental synthesis, we modeled the aspherical nanogel as an ellipsoidal shell of revolution (prolate or oblate) of dry outer principal radii $a_{out,0}$ and $b_{out,0}$, dry inner principal radii $a_{in,0}$ and $b_{in,0}$, swollen outer principal radii a_{out} and b_{out} , and swollen inner principal radii a_{in} and b_{in} .

As in previous work, ^{51,52} we combined the Flory–Rehner theory of swelling of crosslinked polymer networks^{53–55} with the Hertz theory of pair interactions between elastic bodies.⁵⁶ The Flory-Rehner theory combines mixing entropy, polymer-solvent interactions, and elastic free energy to predict the total free energy of a spherical nanogel, As in previous work, 51,52 we combined the Flory-Rehner theory of swelling of crosslinked polymer networks^{53–55}

Hertz theory of pair interactions between elastic bodies.⁵⁶ The Flory-Rehner theory combines mixing entropy, polymer-solvent interactions, and elastic free energy to predict the total free energy of a spherical nanogel,

$$\beta F(\alpha) = N_{\text{mon}} \left[(\alpha^3 - 1) \ln(1 - \alpha^{-3}) + \chi(1 - \alpha^{-3}) \right]$$

$$+ \frac{3}{2} N_{\text{ch}} (\alpha^2 - \ln \alpha - 1), \qquad (1)$$

where $\alpha \equiv a/a_0$ is the swelling ratio, $\beta \equiv 1/(k_BT)$ at temperature T, N_{mon} and N_{ch} are, respectively, the numbers of monomers and crosslinked chains making up the nanogel, and χ is the Flory solvency parameter, associated with polymer-solvent interactions. Defining a chain as a polymer coil spanning two crosslinkers and assuming that each crosslinker connects four chains, the crosslink fraction is $x = 0.5N_{\rm ch}/N_{\rm mon}$. We choose the reference radius of the nanogel to be that in the dry (collapsed) state and assume random close packing of monomers in the dry state with (maximum) volume fraction 0.63. Thus, for a spherical nanogel of dry volume $v_0 = (4\pi/3)a_0^3$

$$N_{\rm mon} = 0.63 \left(\frac{a_0}{r_{\rm mon}}\right)^3,$$
 (2)

where $r_{\text{mon}} \simeq 0.3$ nm is the typical monomer radius. If we would instead assume a different structure of monomers in the dry state, say a hexagonal close-packed (HCP) or face-centered cubic (FCC) crystal with a higher maximum volume fraction of 0.74, then the numbers of monomers N_{mon} and chains N_{ch} appearing in the Flory-Rehner free energy for a given dry radius and crosslink fraction would increase, tending to suppress swelling/deswelling of the nanogels. However, such relatively small quantitative changes in the model would not qualitatively affect the trends observed in the simulations nor our general conclusions.

Swelling of an ellipsoidal nanogel can also be modeled by Eq. (1) with appropriate values of N_{mon} and N_{ch} , assuming isotropic swelling, i.e., equal swelling ratios along the short and long axes: $\alpha \equiv b_{\text{out}}/b_{\text{out},0} = a_{\text{out}}/a_{\text{out},0}$. For a prolate ellipsoid of revolution of dry volume $v_{\text{out},0} = (4\pi/3)a_{\text{out},0}^2 b_{\text{out},0}$ (assuming $a_{\text{out},0} \le b_{\text{out},0}$),

$$N_{\rm mon} = 0.63 \ \frac{a_{\rm out,0}^2 b_{\rm out,0} - a_{\rm in,0}^2 b_{\rm in,0}}{r_{\rm mon}^3}.$$
 (3)

Although based on mean-field approximations that neglect microscopic structure and correlations between monomers making up the polymer network, the Flory-Rehner theory qualitatively captures the freedom of nanogels to swell and deswell.5

Between a pair of spherical nanogels, i and j, with center-tocenter separation r_{ij} , the Hertz theory predicts a pair interaction potential⁵

$$v_H(r_{ij}) = \begin{cases} \varepsilon_{ij} \left(1 - \frac{r_{ij}}{a_i + a_j} \right)^{5/2}, & r_{ij} < a_i + a_j, \\ 0, & r_{ij} \ge a_i + a_j, \end{cases}$$

$$(4)$$

where overlap $(r_{ij} < a_i + a_j)$ implies particle faceting and the amplitude is given by

$$\varepsilon_{ij} = \frac{8}{15} \left(\frac{1 - \nu_i^2}{Y_i} + \frac{1 - \nu_j^2}{Y_j} \right)^{-1} (a_i + a_j)^2 (a_i a_j)^{1/2}, \tag{5}$$

which depends on the elastic properties of the gel through the Young's moduli Y_i and Poisson ratios v_i . Assuming that all particles have equal Poisson ratio v,

$$\varepsilon_{ij} = \frac{8}{15} \frac{Y_i Y_j}{Y_i + Y_j} \frac{(a_i + a_j)^2}{1 - v^2} (a_i a_j)^{1/2}.$$
 (6)

From scaling theory of polymer gels in good solvents,⁵⁸ according to which the bulk modulus scales linearly with temperature and crosslinker density $(Y_i \sim k_B T N_{ch}/a_i^3)$, we have

$$\beta \varepsilon_{ij} = C \frac{N_{\text{ch}}}{a_i^3 + a_j^3} (a_i + a_j)^2 (a_i a_j)^{1/2}.$$
 (7)

To calibrate the model with experiment, we chose the proportionality constant $C \simeq 10$, as in our previous application of this model to describe the deswelling of microgels in crowded suspensions.⁵⁹ The coefficient C in Eq. (7) is introduced as an empirical prefactor in the amplitude of the Hertz pair potential to account for microscopic properties of the nanogels, such as crosslink distribution, that are not accounted for in either the Hertz model or the scaling theory. The lower the value of C the lower the effective Young's modulus and thus the lower the energetic penalty of particle overlaps, corresponding to softer nanogels. The specific choice does not qualitatively affect the trends observed in the simulations and thus does not influence our general conclusions. Comparisons of the coarse-grained Hertz elastic theory with microscopic models of nanogels^{60,61} demonstrate that the Hertz pair potential is reasonably accurate for modest overlaps (faceting) of nanogels corresponding to $v_H(r) \sim 5k_BT$.

In principle, interactions between the ellipsoidal and spherical nanogels could also be modeled via the Hertz elastic theory. For simplicity and to somewhat amplify the crowding effects, we assumed the ellipsoidal nanogel to be impenetrable to the spherical nanogels, thus modeling ellipsoid–sphere interactions by a hard contact pair potential, infinite for overlapping particles and otherwise zero. Denoting by \mathbf{r}_i the position vector of the center of spherical nanogel i and by \mathbf{R} the position of the center of the ellipsoidal nanogel, the total internal energy associated with pair interactions among all the nanogels is then given by

$$U_{\text{pair}} = \sum_{i < j=1}^{N} \nu_H(r_{ij}) + \sum_{i=1}^{N} \nu_{\text{hard}}(\mathbf{r}_i, \mathbf{R}),$$
(8)

where for each sphere–sphere interaction the appropriate amplitude is taken from Eq. (7), while for each ellipsoid–sphere interaction the pair potential v_{hard} is either infinity or zero, depending on whether or not the two particles overlap.

To further incorporate the additional freedom of an ellipsoidal nanogel to change its shape, we introduced an elastic energy due to deformation by stretching of the long axis,

$$U_{\text{def}} = \frac{1}{2}k(b_{\text{out}} - b_{\text{out},r})^2,$$
 (9)

where k is a Hookean "spring constant" and $b_{\text{out},r}$ is the major principal radius of the fully swollen, uncrowded (reference) ellipsoid. Relating k to the Young's modulus Y of the ellipsoidal nanogel yields

$$k \propto \frac{A_e}{b_{\text{out}}} Y \propto \frac{A_e}{b_{\text{out}}} \frac{N_{\text{ch}}}{V_e},$$
 (10)

where A_e and V_e are the cross-sectional area and volume of the ellipsoidal shell. For sufficiently large values of k, the ellipsoidal nanogel must closely retain its uncrowded shape, while for lower values, the ellipsoid can more readily fluctuate in shape and adjust to its crowded environment. In practice, we chose the prefactor in the proportionality [Eq. (10)] to calibrate the behavior of the model to the experimental observations of shape deformation.

Finally, combining Eqs. (1), (8) and (9) yields the total energy of the system,

$$U_{\text{tot}} = \sum_{i=1}^{N} F_{\text{sphere}}(\alpha_i) + F_{\text{ellipsoid}} + U_{\text{pair}} + U_{\text{def}}, \tag{11}$$

where F_{sphere} and $F_{\text{ellipsoid}}$ represent the Flory–Rehner free energy [Eq. (1)] for spherical and ellipsoidal nanogels.

G. Simulation methods

Coding our Monte Carlo simulations in the Open Source Physics Library, 62 we placed N spherical nanogels and one ellipsoidal nanogel in a cubic box of volume V to which periodic boundary conditions were applied in all dimensions. Trial moves were made in accordance with the standard Metropolis algorithm 63,64 with acceptance probability

$$\mathcal{P}_{acc} = \min\{\exp[-\beta(\Delta U_{tot})], 1\}, \tag{12}$$

where ΔU_{tot} is the resultant change in total energy [Eq. (11)]. For all of the nanogels, a trial move combined a trial displacement and trial change in swelling ratio. For the ellipsoid, a trial move also included a trial rotation and shape change. Trial rotations were performed by changing the orientation of the ellipsoid, defined by a unit vector $\hat{\mathbf{u}}$ aligned with the major axis via addition to $\hat{\mathbf{u}}$ of a randomly generated vector of magnitude $\ll 1$. In this way, the ellipsoidal nanogels were allowed to rotate freely in three dimensions. Trial shape changes were generated in a manner that preserved the particle's dry volume under the assumption that, regardless of the swollen nanogel's shape, the monomers in the dry (collapsed) state remained in a random close-packed configuration. Trial moves that resulted in ellipsoid-sphere overlaps were automatically rejected. Such overlaps were diagnosed using the same algorithm as in our previous work on crowding of polymers by colloids or nanoparticles. 65-69 This algorithm determines the shortest distance between the center of the sphere and the surface of the ellipsoid, which involves computing roots of a sixth-order polynomial.7

To initialize the system, we distributed the spherical nanogels over the sites of a face-centered cubic (FCC) lattice and placed the ellipsoid at an interstitial site. We chose this initialization so as to maximize the nearest-neighbor separation and avoid any initial overlaps of particles. At the relatively low concentrations studied, the initial lattice structure immediately melts upon commencing the simulation. In previous studies of spherical microgels⁴⁷ in which

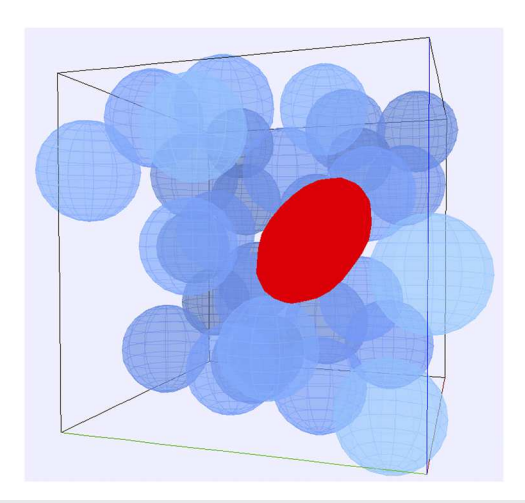


FIG. 1. Snapshot from a Monte Carlo simulation, showing a cubic box containing one ellipsoidal nanogel (red particle), which is free to change its position, size, shape, and orientation, immersed in a crowded environment of spherical nanogels (blue particles), which can change only their positions and sizes.

we initialized an ideal-gas version of the system in random configurations and then gradually switched on interparticle interactions, we confirmed that the initial configuration does not affect the final equilibrium properties at concentrations in the fluid phase.

On running a simulation, we performed independent Monte Carlo (MC) steps, a step being defined as one trial move for every particle in the system. As the particles moved and adjusted their internal degrees of freedom, we updated the Hertz pair potential amplitudes on the fly according to Eq. (7). After cycling through many trial moves and thus sampling many configurations, the system approached equilibrium distributions of spherical nanogel size and of ellipsoidal nanogel size and shape, ultimately minimizing the system's Helmholtz free energy at fixed N, V, and T. Figure 1 shows a snapshot from a typical simulation with N = 32 spherical nanogels.

III. RESULTS AND DISCUSSION

SANS with contrast variation has been largely used to directly probe changes in the shape and architecture of compressible nanogels in crowded environments. 27,59,71-73 Here, we use the socalled tracing-method in which a few hydrogenated nanogels are mixed with a majority of deuterated nanogels that are contrastmatched by a proper mixture of water and heavy water.²⁷ The hydrogenated anisotropic (ellipsoidal) nanogels (HAN) were embedded in a matrix of either spherical or virtually identical ellipsoidal nanogels synthesized using a deuterated monomer, C₆H₄D₇NO. We note that all the nanogels used in this study have been synthesized adding a 5 mol % BIS during the precipitation polymerization. Recently, we have shown that when hollow nanogels are compressed using an osmotic stress solution, the stiffness of their polymeric network is comparable to the one of regular nanogels synthesized with the same amount of BIS.⁷⁴ This ensures that all the polymeric networks of the nanogels used here present a similar resistance to compression.

The anisotropic shape of the HAN under dilute conditions was verified using both dynamic light scattering and transmission

electron microscopy; see Fig. 7 in Appendix C. We refer to the deuterated spherical and anisotropic nanogels as deuterated spherical nanogels (DSN) and deuterated anisotropic nanogels (DAN), respectively.

In neutron scattering, due to the differing atomic scattering lengths of hydrogen and deuterium,⁷⁵ the use of a proper mixture of water and heavy water allows us to contrast-match the contribution of the deuterated particles to the measured background intensities.²⁷ As a result, only the hydrogenated anisotropic nanogels are visible during the SANS experiments. The measured intensities are, therefore, directly proportional to the form factor of the hydrogenated nanogels. The analysis of this part of the scattering signal allows us to determine all the information on the shape and characteristic lengths of the HAN and how these quantities changes at different sample concentrations. In other words, these measurements allow us to probe how the particle architecture changes in crowded environments.

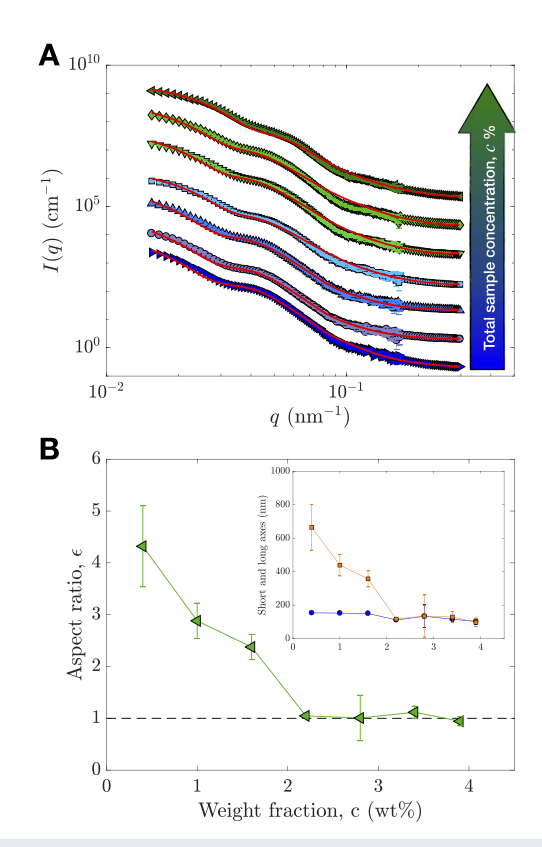


FIG. 2. (a) Small-angle neutron scattering intensities, I(q), vs scattering vector, q, relative to the hydrogenated anisotropic nanogels (HAN) measured in a matrix of deuterated spherical nanogels (DSN) using contrast variation techniques (tracingmethod). The total sample concentrations are $c=0.400\pm0.003$ (right-pointing triangles), 0.92 ± 0.04 (circles), 1.30 ± 0.07 (up-pointing triangles), 2.18 ± 0.04 (squares), 2.81 ± 0.02 (down-pointing triangles), 3.30 ± 0.02 (diamonds), and 4.10 ± 0.02 wt% (left-pointing triangles). All measurements were performed at $T=20.0\pm0.1\,^{\circ}\mathrm{C}$. (b) Aspect ratio, ε , as a function of the sample concentration, c. Inset: variation of the lengths of the short axis (circles) and long axis (squares) as a function of sample concentration c. The values are obtained from the fits of the data in (a) using the model of Ref. 44.

TABLE I. Concentration, c, aspect ratio, ε, length of the short semi-axis, R_{SANS} , internal and external fuzziness ($σ_{in}$ and $σ_{out}$, respectively), polydispersity, PD, $χ^2$ obtained from the fitting of the scattering data, and generalized volume fraction of the spherical nanogels composing the matrix, ζ.

c (%)	ε	R _{SANS} (nm)	σ_{in} (nm)	σ_{out} (nm)	PD (%)	χ^2	ζ
0.400 ± 0.003	4.3 ± 0.8	154 ± 4	18.9 ± 0.2	6.7 ± 0.4	15	12.2	0
0.92 ± 0.04	2.9 ± 0.3	152 ± 65	18.2 ± 0.3	7.1 ± 0.5	15	6.80	0.15 ± 0.01
1.30 ± 0.07	2.4 ± 0.2	150 ± 48	18.5 ± 0.3	6.6 ± 0.5	15	8.65	0.26 ± 0.01
2.18 ± 0.04	1.01 ± 0.02	111 ± 3	18.4 ± 0.2	0.2	23	11.0	0.52 ± 0.02
2.81 ± 0.02	1.0 ± 0.4	134 ± 126	13.2 ± 5.0	3.9 ± 0.3	23 ± 3	36.1	0.71 ± 0.02
3.30 ± 0.02	1.1 ± 0.1	116 ± 16	17.5 ± 1.7	0.2	23 ± 2	49.6	0.85 ± 0.02
4.10 ± 0.02	0.94 ± 0.09	103 ± 17	13.8 ± 1.8	0.2	21 ± 2	29.5	1.09 ± 0.03

In previous work, we showed that to properly fit the experimental SANS data and reproduce the nanogel architecture, a model accounting for the internal cavity, the particle anisotropy, and the internal and external fuzziness is needed.⁴⁴ A complete model description is given by Eqs. (1)-(7) in Nickel et al.44 and in the supplementary material of the same publication. To reduce the number of parameters, the size polydispersity was fixed to 15%. This value was obtained in our previous study by fitting the scattering curves of diluted suspensions of ellipsoidal hollow nanogels with Eqs. (1)–(7) in Ref. 44. Since the ellipsoidal nanogels have been synthesized with the very same procedure used by Nickel et al., 44 the size polydispersity of the overall particles is considered to be the same as determined in that study. We note that in our model, we exclude differences in the polydispersity of the different axes since this is beyond the SANS resolution. Nevertheless, the analysis of transmission electron microscopy (TEM) micrographs, similar to the one shown in Figs. 7 and 8, does not show a large difference in the shape and/or aspect ratio dispersity, and therefore, the use of 15% for the size polydispersity of the nanogels is reasonable.

In Fig. 2(a), the bottom curve shows the measured SANS intensity, I(q), as a function of the scattering vector q (right-pointing triangles) measured for a sample composed of anisotropic hydrogenated nanogel at a concentration c=0.4 wt. %. The red curve represents the data fit using our model. Table I reports the values of the fitting parameters. The inset of Fig. 2(b) shows the length of the short (circle) and long (squares) axes. An aspect ratio of 4.3 ± 0.8 is obtained, which confirms the anisotropic shape observed within the TEM image (Fig. 7).

A. Hydrogenated anisotropic nanogel in spherical matrix

The other curves in Fig. 2(a) correspond to samples composed of a fixed concentration of HAN, $c_{HAN}=0.400\pm0.003$ wt. %, embedded in a matrix of deuterated spherical nanogels synthesized with the same amount of crosslinkers. The concentration of DSN increases from $c_{DSN}=0$ wt. % (bottom curve, right-pointing triangles) to 3.70 \pm 0.02 wt. %, implying that the total sample concentration is between $c=0.400\pm0.003$ and 4.10 ± 0.02 wt. %. For the spherical nanogels, values of the suspension viscosity at $c_{DSN}\lesssim0.4$ wt. % are fitted with the Einstein–Batchelor equation to obtain a conversion constant between the mass concentration and the generalized volume fraction ζ , defined as the volume fraction of

fully swollen nanogels in solution. For the DSN, the values of the conversion constant are 29.4 ± 0.6 , ⁴⁶ implying that ζ of the spherical nanogels lies in the range from 0.15 to 1.09 (see Table I).

It is clear that with increasing ζ of the matrix, both the decay of I(q) at low-q and the minimum–maximum are shifted to higher q. This trend corresponds to a decrease in size and/or change in the characteristic lengths of the HAN.^{27,71,72} To have a more quantitative description of the changes, we also fit these data with our model. The red curves in Fig. 2(a) represent the data fit. Table I reports the values of the fitting parameters and the corresponding errors.

The internal fuzziness is conserved at all studied concentrations, indicating that the nanogels maintain their cavity. This behavior is in agreement with the behavior of spherical hollow nanogels embedded in a matrix of either regular or hollow nanogels. In contrast, the outer fuzziness decreases with increasing DSN concentration. In addition, this fact is consistent with the behavior of the fuzzy shell for spherical nanogels in crowded environment. In addition, this fact is consistent with the behavior of the fuzzy shell for spherical nanogels in crowded environment. In addition, this fact is consistent with the behavior of the fuzzy shell for spherical nanogels show a fuzzy outer shell until the matrix of DSN has a $\zeta \lesssim 0.74$ ($c \lesssim 3$ wt. %), i.e., above the maximum volume fraction of hard spheres in three dimensions. Above this value, the external shell is almost completely collapsed. Consequently, one can neglect the role of the existing dangling chains at the nanogel periphery since they are collapsed on the particle surface as soon as the nanogel concentration and, therefore, the suspension osmotic pressure increases.

More interestingly, the length of the long semi-axis is decreasing with increasing DSN concentration, indicating deswelling of the nanogels (see Appendix A for the calculation of the short semiaxis R_{SANS}). The inset in Fig. 2(b) shows the evolution of the short (circles) and long (squares) semi-axes as a function of c. The data clearly demonstrate that the ellipsoidal nanogels are compressed with increasing sample concentration. Even more interesting is that for c > 2 wt. %, both the axes have virtually the same length, i.e., the ellipsoidal particles become spherical as also indicated by the evolution of the aspect ratio ε as a function of c, shown in Fig. 2(b). The concentration *c* above which the HAN become more spherical corresponds to a ζ for the matrix of DSN of 0.6, i.e., just above the lowest volume fraction at which glass transition happens for hard spheres, $\phi = 0.58$. We also note that the DSN concentration is in the proximity of the random close-packing fraction of hard spheres in bulk, $\phi_{rcp} = 0.63$. This observation indicates that together with osmotic effects that lead to an osmotic deswelling,^{27,78,79} also the particle-to-particle contacts can produce some faceting of the HAN

as already observed for spherical nanogels using both computer simulations ^{61,80} and super-resolved fluorescence microscopy. ^{9,21}

In contrast to low concentrations, to obtain better fits, for c > 2 wt. % ($\zeta \gtrsim 0.6$), the parameter representing the size polydispersity is left free to change and an evolution from 15% up to $\approx 20\%$ is observed. The increase in the parameter describing the size polydispersity when fitting scattering data relative to soft deformable objects in crowded environments has often been related to the potential faceting of the particles. 11,47,48,81 This fact has been finally demonstrated by combining computer simulation of faceted colloids and SANS data of nanogels in crowded environments. 24

Now, if the aspect ratio of the ellipsoidal nanogels decreases to ≈ 1 with increasing ζ of the matrix of DSN, it means that their form factor is comparable to the form factor of spherical nanogels. Under these conditions, a suspension of DSN and a suspension of a mixture of DSN and few collapsed HAN ($c_{HAN}=0.4$ wt.%) have the same structure factor and nearest-neighbor distance, d_{nn} , at the same ζ . Therefore, we can divide the intensity of the two concentrated suspensions for the form factor of the DSN and obtain the suspension structure factors that must have the structural peaks at approximately the same q-values. In contrast, if the ellipsoidal nanogels maintain their shape, once we divide the I(q) measured for a concentrated suspension by the P(q) of a suspension of diluted spheres, the structural peaks do not appear due to the contribution of the ellipsoids in the low and middle q-range of I(q).

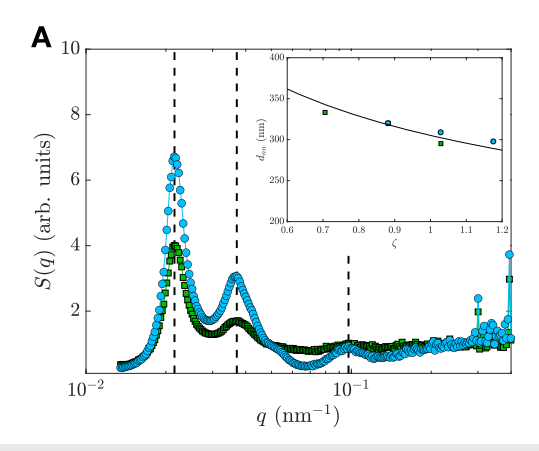
To check this hypothesis using SAXS, we measured concentrated solutions of pure DSN and mixture of DSN and HAN in the same solvent used for the SANS experiments with contrast variation. Indeed, x rays do not distinguish between hydrogen and deuterium, and all the particles and, therefore, the suspension's structure factor contribute to the measured I(q). The values of ζ of the DSN lie in range from 0.35 to 1.03. As an example, in Figs. 3(a) and 9, we show the structure factors of a suspension composed of only deuterated spherical nanogels (light blue circles) and a mixture of the same deuterated spherical nanogels with protonated ellipsoidal

nanogels (green squares) with a concentration of 0.4 wt. %. The generalized volume fraction of the DSN is $\zeta = 0.88 \pm 0.02$ [Figs. 3(a)] and $\zeta = 1.03 \pm 0.02$ (Fig. 9).

The structure factors are obtained by dividing the measured intensities by the intensity of a dilute suspension of the spherical nanogels, which is proportional to the particle form factor. As indicated by the dashed lines, the structural peaks of the S(q)s of the two measured solutions are in the exact same position. This indicates that the arrangement of the particles in the two samples is exactly the same. Furthermore, the inset of Fig. 3(a) shows the values of the nearest-neighbor distance, d_{nn} , as a function of the values of ζ of the DSN of solutions of deuterated spherical nanogels (light blue circles) and of the mixtures of DSN and HAN (green squares). We obtained d_{nn} from the values of q corresponding to the first structural peak of S(q). ^{72,82} Both the suspensions of pure DSN and the mixtures of DSN and HAN have virtually the same d_{nn} , which decreases according to the behavior expected for an isotropic deswelling, $\zeta^{-1/3}$ (solid line). 72,73,80 Furthermore, Fig. 10(a) corresponds to a c_{DSN} where the aspect ratio of the ellipsoid is already ≈1 (Fig. 2) and still a reliable structure factor can be obtained.

In contrast, in Figs. 3(b) and 10(b), we show the structure factors of samples for $c_{DSN} \le 2.4$ wt. % ($\zeta \lesssim 0.70$). These data show that at low c_{DSN} , the S(q) cannot be obtained by dividing the I(q) by the measured form factor of spheres. As mentioned above, this indicates that the ellipsoidal nanogels retain their anisotropic shape. Indeed, Figs. 3(b) and 10(b) correspond to value of the aspect ratio larger than one.

Our SAXS data further support the SANS observation. Once the HAN particles are embedded in a matrix of spherical nanogels at $\zeta \gtrsim 0.70$, the structure factors and nearest-neighbor distance of these mixtures are exactly the same as those measured for suspensions composed of spherical particles only. This result and the direct determination of the aspect ratio using SANS and contrast variation imply that the ellipsoidal nanogels become spherical and fit into the arrangement of the matrix composed of spheres.



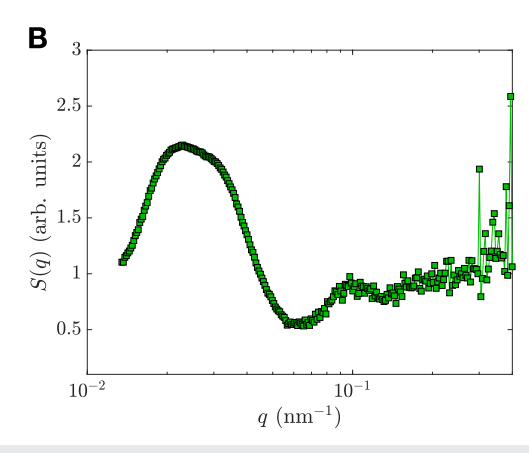


FIG. 3. (a) Small-angle x-ray scattering structure factor, S(q), of suspensions composed of only deuterated spherical nanogels (light blue circles) at $c_{DSN}=3$ wt. % and a mixture of the same deuterated spherical nanogels at $c_{DSN}=3$ wt. % with protonated ellipsoidal nanogels (green squares) with a concentration of 0.4 wt. %. Dashed lines highlight the peak positions. Inset in A: values of the nearest-neighbor distance, d_{nn} , vs generalized volume fraction of the spherical nanogels, ζ . Data correspond to the solutions of deuterated spherical nanogels (light blue circles) and to the mixtures of deuterated spherical nanogels and protonated ellipsoidal nanogels with a concentration of 0.4 wt. % (green squares). The solid curve represents the expected behavior of d_{nn} in case of isotropic deswelling of spherical nanogels, $\zeta^{-1/3}$. (b) S(q) of a sample composed by a mixture of deuterated spherical nanogels, $c_{DSN}=1.8$ wt. %, and protonated ellipsoidal nanogels with a concentration of 0.4 wt. %.

B. Simulation results

To complement the experiments and help to rationalize the observations, we developed and applied Monte Carlo (MC) simulation methods to model an ellipsoidal nanogel immersed in a crowded environment of spherical nanogels. As input to our simulations, we chose the system parameters summarized in Table I. These parameters ensure that the geometries (sizes and shapes) of the swollen nanogels match as closely as possible to the experimental observations. After an initial equilibration phase of 10⁴ MC steps, we collected statistics on principal radii of the ellipsoidal nanogel for an additional 10⁵ steps. To determine statistical uncertainties, we performed five independent runs. Runs with fewer particles confirmed that finite-size effects are negligible.

Figure 4 shows our simulation results for the mean aspect ratio $\varepsilon \equiv \langle b_{\rm out}/a_{\rm out} \rangle$ of the ellipsoidal nanogel over a range of generalized volume fraction ζ of the spherical nanogels for the system parameters in Table II. As ζ varies from 0 to 1.3, the dry volume fraction ϕ_0 varies in proportion from 0 to about 0.03. The error bars, computed from standard deviations over the five independent runs, represent statistical uncertainties in the data due to fluctuations. At the lowest nanogel concentrations (i.e., lowest values of ζ), the ellipsoidal nanogel rarely interacts with the spherical nanogels and thus is free to adopt its uncrowded size and shape distributions. The relatively large error bars in this case reflect the relative ease with which the ellipsoid may deform its shape for these system parameters. With increasing concentration (increasing ζ), the mean aspect ratio tends to decrease and the error bars narrow. This trend demonstrates the growing influence of crowding by the spherical nanogels on the ellipsoidal nanogel's shape, driving its average shape toward spherical and limiting the range of fluctuations. Interestingly, we find that crowding does not significantly affect the volume of the swollen ellipsoidal nanogel—a somewhat surprising result, since only the dry volume was constrained to be constant. Evidently, for these system parameters, the energetic cost of swelling/deswelling of the gel significantly exceeds the cost of elastic deformations, which enable the shape to change in response to crowding.

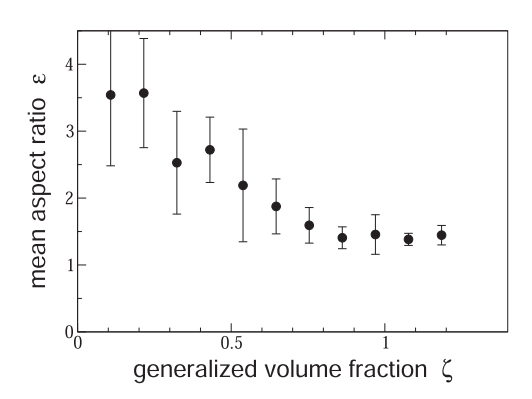


FIG. 4. Mean aspect ratio $\varepsilon \equiv \langle b_{\text{out}}/a_{\text{out}} \rangle$ of an ellipsoidal nanogel vs generalized volume fraction ζ of spherical nanogels for the system parameters in Table II, showing the tendency of the ellipsoidal nanogel to approach a spherical shape with increasing crowding by spherical nanogels.

TABLE II. System parameters used in Monte Carlo simulations: number of spherical nanogels N, dry radius of spherical nanogels a_0 , dry outer principal radii of ellipsoidal nanogel, $a_{\text{out},0}$ and $b_{\text{out},0}$, dry inner principal radii of ellipsoidal nanogel, $a_{\text{in},0}$ and $b_{\text{in},0}$, crosslink fraction $x=0.5N_{\text{ch}}/N_{\text{mon}}$ of both types of nanogel, and Flory solvency parameter χ .

N	<i>a</i> ₀ (nm)	a _{out,0} (nm)	bout,0 (nm)	<i>a</i> _{in,0} (nm)	$b_{\rm in,0}~({\rm nm})$	х	<i>X</i>
108	60	40	120	30	100	5 × 10	⁻⁴ 0

C. Hydrogenated anisotropic nanogel in ellipsoidal matrix

Next, we studied the behavior of the anisotropic particles embedded in a matrix of virtually identical but deuterated anisotropic nanogels (DAN). Similar to DSN, the DAN are matched by a mixture of water and heavy water in the SANS experiments and only the structural information of HAN determines the scattering intensity. Figure 5 shows the scattering data of HAN embedded in a matrix of DAN with concentrations $c_{DAN} = 0$, 3.9 \pm 0.1, and 5.5 ± 0.5 wt.%. The first minimum remains at a similar position with an increase in DAN concentration. However, we observe an increase in the intensity both of the smeared minimum $(q \approx 3 \cdot 10^{-2} \text{ nm}^{-1})$ and in the mid-q region, $7 \cdot 10^{-2} \text{ nm}^{-1} < q$ $< 2 \cdot 10^{-1}$ nm⁻¹. Those changes are different with respect to the changes in the I(q)s observed once the HAN are embedded in the matrix of deuterated spheres. To quantify this difference and describe precisely the shape and architecture of anisotropic particles in a matrix of concentrated anisotropic particles, we fit the data using our model (solid lines in Fig. 5).

The one-shell ellipsoidal model suitable to fit HAN in dilute dispersions and in the environment of spherical nanogels cannot reproduce the experimental data, especially in the \min -q region (see Fig. 11 in Appendix E). Therefore, we included a second shell in our model as reported in the literature.⁴⁴ Even in this case, the parameter describing the size polydispersity was kept constant at 15%

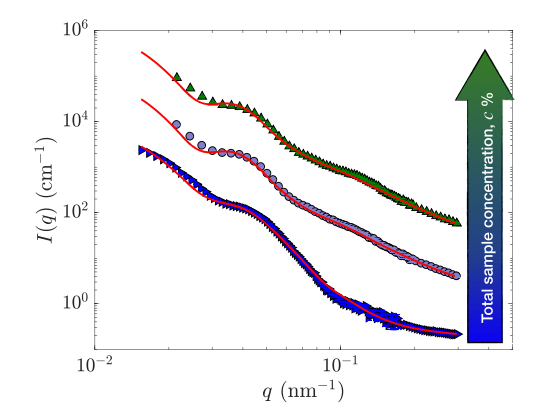


FIG. 5. Small-angle neutron scattering intensities, I(q), vs scattering vector, q relative to the hydrogenated anisotropic nanogels (HAN) measured in a matrix of deuterated anisotropic nanogels (DAN) using contrast variation techniques (tracing-method). The sample concentrations are $c = 0.400 \pm 0.003$ (right-pointing triangles), 4.2 ± 0.1 (circles), and 5.9 ± 0.5 wt. % (up-pointing triangles). All measurements were performed at $T = 20.0 \pm 0.1$ °C.

TABLE III. Aspect ratio, short semi-axis, inner and outer fuzziness, polydispersity, and χ^2 obtained from the fitting of the scattering data of hydrogenated anisotropic nanogels mixed with deuterated anisotropic nanogels.

c (%)	ε	R _{SANS} (nm)	σ_{in} (nm)	σ _{out} (nm)	PD (%)	χ^2
0.400 ± 0.003	4.3 ± 0.8	154 ± 4	18.9 ± 0.2	6.7 ± 0.4	15	12.2
4.2 ± 0.1	9.2 ± 1.9	135 ± 15	15.1 ± 1.0	3.8 ± 1.2	15	4.4
5.9 ± 0.5	9.0 ± 1.2	130 ± 17	15.0 ± 1.1	2.9 ± 1.3	15	6.9

to reduce the number of fit parameters. The values of the parameters as obtained from the data fits and the corresponding errors are reported in Table III.

Despite the structural changes in the external fuzzy shell, the most important result from the fits is that in contrast to the case where the matrix is composed of spherical nanogels, the increase in concentration of anisotropic particles leads to a significant increase in the aspect ratio of the hydrogenated anisotropic nanogels (Table III). This trend is a consequence of the increase in the length of the long axis and the corresponding small decrease in the length of the short axis. Therefore, not only the overall shape of the nanogels remains anisotropic, but the anisotropy is even enhanced by the increase in sample concentration.

The picture that emerges from the small-angle neutron and x-ray scattering data and the Monte Carlo simulations is that anisotropic nanogels can adapt their size and shape—including the passage from an anisotropic shape to a spherical shape—as a consequence of the concentration and the architecture of the nanogels composing the matrix in which they are embedded. Such a difference in response of anisotropic soft nanogels depending on the shape of the particle composing the matrix can be rationalized by considering the work needed to deswell isotropically or deform an ellipsoidal nanogel.

Let us start by considering the overlap between a sphere and an ellipsoid, denoting the extent of the overlap by h_d . As mentioned, nanogels can isotropically deswell due to osmotic pressure effects, ^{27,28} and this can be used to directly measure the nanogel's resistance to compression. ^{74,83} The work needed to isotropically deswell a nanogel of volume $\Delta V(h_d)$ can be written as

$$W_s = \Pi_{in} \Delta V(h_d), \tag{13}$$

where Π_{in} is the osmotic pressure inside the nanogel, which depends on both the crosslinking of the polymeric network and the quality of the solvent, according to the Flory–Rehner theory of polymer networks. 54,55,84

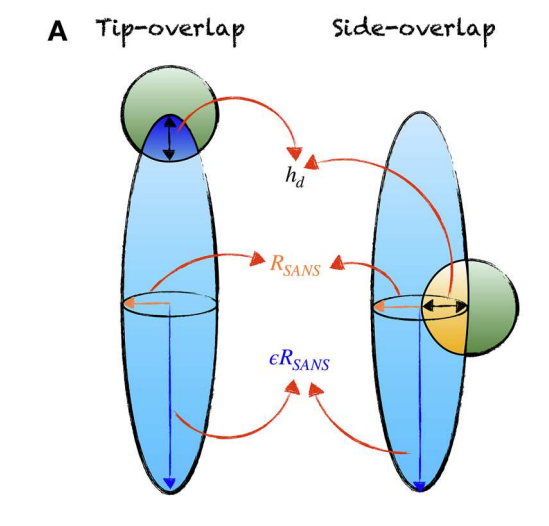
Similarly, the work needed to deform a nanogel with Young's modulus E that overlaps with another is

$$W_d = \int_0^{h_d} F(h) dh \propto E \Delta V(h_d), \tag{14}$$

with F(h) being the force required to compress the ellipsoidal nanogel by a depth h_d . This force is calculated from the profile of the object, assumed to be in elastic contact with the sphere, and the interaction is approximated using a Hertzian model. Here In both cases for Eqs. (13) and (14), the work to change the volume corresponding to a penetration depth of h_d is proportional to the volume

of the overlap between the sphere and the ellipsoid. This means that the work to achieve both deformation and isotropic deswelling increases with increasing $\Delta V(h_d)$. Now, let us limit ourselves to the simple cases of overlap of a sphere with the ellipsoid along two preferential directions: the long and the short axes. In Fig. 6(a), the sketches of the ellipsoid are scaled to the value of the long and short axes reported in Table I for the HAN in the dilute case, $c=0.400\pm0.003$ wt.%.

Assuming the sphere penetrates the ellipsoid in both directions by the same depth, h_d , we can compute the volume of the overlap in



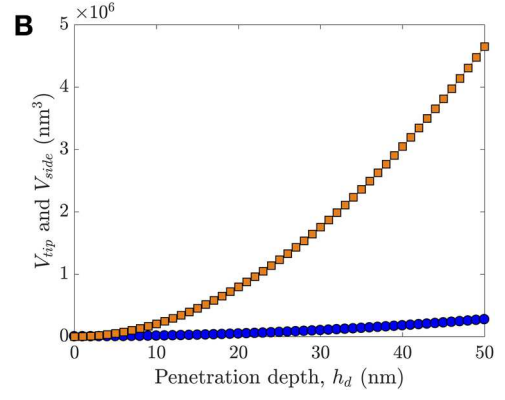


FIG. 6. (a) Sketch of the overlap between a sphere and an ellipsoid along the longand short-axis direction, tip-overlap and side-overlap, respectively. (b) Volume of overlap, V_{tio} (circles) and V_{side} (squares), vs lengths of overlap, h_d .

the cases of tip- and side-overlap. The volume of an ellipsoidal dome of high h_d is

$$V = \frac{\pi ab}{3c^2} h_d^2 (3c - h_d). \tag{15}$$

For an ellipsoid with axes $a = b = R_{SANS}$ and $c = \varepsilon R_{SANS}$, the overlap for the tip- and side-overlap can be written as

$$V_{tip} = \frac{\pi}{3\varepsilon^2} h_d^2 (3\varepsilon R_{SANS} - h_d), \tag{16}$$

$$V_{side} = \frac{\varepsilon \pi}{3} h_d^2 (3R_{SANS} - h_d). \tag{17}$$

In Fig. 6(b), the values of V_{tip} (blue circles) and V_{side} (orange squares) are plotted as a function of increasing penetration depth. As can be seen, except for moderate values of h_d , the volume of the overlap from the side (orange squares) is always significantly larger than the volume of the overlap in the direction of the longer axis (blue circles). This means that the work to deswell or rearrange the polymer in the case of a tip-overlap is much smaller than the work needed to deform or deswell the polymer in a side-overlap. As a consequence, the deswelling or deformation of the ellipsoid tips is energetically less penalizing, which can explain the passage from the anisotropic to spherical shape of the HAN once embedded in the matrix of spherical nanogels. We note that here the overlap proceeds in both directions with the same penetration depth. Alternatively, one may set the two penetrations to cover the same "overlap volume," and therefore, the tip-overlap would lead to a larger penetration depth with respect to the side-overlap. However, the possibility of detecting such different penetration depths is beyond the SANS/SAXS resolution. A more detailed interpretation of our scattering results can be achieved in the future by combining our experimental results with computer simulations of realistic anisotropic nanogels to probe the microscopic aspects of the nanogel-to-nanogel interaction.

Interestingly, a similar behavior has been reported for linear polymer coils in crowded environments of hard-sphere-like colloids, where the polymers are modeled as ellipsoids that fluctuate in shape according to the statistics of random walks. ^{65,67} Similar to our experimental results, the computer simulations conducted on these systems reveal that with increasing the concentration of the spheres in the matrix, the ellipsoid approaches a spherical shape.

The influence of a crowded environment of anisotropic nanogels on the shape of an initially ellipsoidal nanogel differs completely from the influence of a concentrated environment of spherical nanogels. We propose that this difference can be rationalized considering that anisotropic particles can form ordered phases in solution. We observe ordering already in the uncompressed state within the TEM images of HAN (see Figs. 7 and 8). A similar behavior is also well documented in the literature for a variety of other anisotropic grafted nanoparticles. ^{33,85,86}

Furthermore, previous studies at interfaces showed that such ordering is increased for similar nanogels with an increase in surface pressure.³⁴ Hence, it is reasonable that the ellipsoids orient themselves in the same direction, leading to a larger contact area between the sides of the ellipsoids compared to their tips. Depending on this arrangement, the overlap between the ellipsoid tips might be negligible while the side-to-side overlap remains still present and the ellipsoid responds by compressing along the short-axis direction.

IV. CONCLUSIONS

Among many soft colloidal systems, nanogels are the only ones that are known to exhibit a self-healing mechanism, whereby defects can selectively deswell depending on the particles' environments. ^{25,26} As a consequence, nanogel solutions with polydisperse or bimodal size distribution can decrease their size disparities. ^{7,24,27} This self-healing mechanism has important effects on the phase behavior of the solutions. For instance, large nanogels with a size ratio of 1.5 can spontaneously deswell and crystals can form without the presence of defects or dislocations. ²⁷ This phenomenon is determined by the increase in osmotic pressure of the solution due to the counterion clouds surrounding both neutral or ionic nanogels. ^{27,28,79,87}

In this study, the behavior of anisotropic nanogels in crowded environments is investigated. The characteristic lengths of the ellipsoidal nanogels are directly determined measuring their form factors as a function of increasing concentration by means of small-angle neutron scattering with contrast variation. The crowding is exerted by either spherical nanogels or ellipsoidal nanogels with a comparable aspect ratio. The fitting of the SANS data, and the structure factors of the samples, measured by means of SAXS, highlight that once the ellipsoidal nanogels are embedded in a matrix of spherical ones, they decrease their aspect ratio with increasing the sample concentrations. This experimental observation is confirmed by computer simulations of a single ellipsoidal nanogel embedded in a matrix of spherical one.

In contrast, the data collected on solution of ellipsoidal nanogels in a matrix of ellipsoidal nanogels indicate that in this case, the aspect ratio increases with increasing sample concentration. In other words, once the ellipsoidal nanogels are embedded in a matrix of spheres, they become spherical while when embedded in a matrix of isotropic particles they become more anisotropic. By considering the different volumes of the overlap between a sphere and an ellipsoid, these changes in the shape are rationalized in terms of the differences in work needed to produce a deformation to change the aspect ratio. The fact that our nanogels are hollow—an inevitable consequence of how anisotropic nanogels are currently obtained—might affect the extent of isotropic deswelling. We have shown that hollow spherical nanogels strongly deswell already at lower applied osmotic stresses with respect to regular nanogels synthesized with comparable amount of crosslinker agents.⁷⁴ However, similar qualitative trends should also apply to non-hollow ellipsoidal nanogels of comparable size, which will be more resistant to compression due to the absence of the cavity but will be subject to the same geometrical constraints.

Our study opens the path for future research using soft colloids to further clarify what is the role of softness and how this quantity can be defined for anisotropic colloids. Further experiments are needed to determine the phase behavior of mixture of ellipsoidal and spherical colloids. Furthermore, by means of rheology and combining it with scattering techniques, the observed changes in the shape has to be observed in solution under flow. Another aspect that must be investigated is the effect of the changes in the shape on the maximum packing fraction these soft ellipsoid can reach in solution, and compare it with what has been observed for a hard ellipsoid. 31,32,88 To better rationalize the experimental observation, it is also desirable to further develop computer simulations able to

realistically approximate ellipsoidal nanogels as it has been performed for spherical ones.^{60,80} These computer simulations should also shed light on the best approximation for the interaction potential between soft anisotropic colloids and verify if the assumption of an Hertzian potential is reasonable.^{8,61}

ACKNOWLEDGMENTS

Financial support was provided by the Deutsche Forschungs-gemeinschaft within SFB 985—Functional Nanogels and Nanogel Systems (Project No. 191948804). The work of ARD was supported by the National Science Foundation (Grant No. DMR-1928073). The small-angle neutron scattering data were measured using the D11 instrument at the Institut Laue-Langevin (ILL), Grenoble, France. The SAXS measurements were performed on the CoSAXS beamline at MAX IV (Lund, Sweden) under the proposal 20200777. The research conducted at MAX IV, a Swedish national user facility, is supported by the Swedish Research council under contract 2018-07152, the Swedish Governmental Agency for Innovation Systems under Contract No. 2018-04969, and Formas under contract 2019-02496. The Authors thank M. Brugnoni for the synthesis of the spherical deuterated nanogels and P. Mota-Santiago, F. M. Schulte, and S. Bochenek for the help during the SAXS measurements.

AUTHOR DECLARATIONS

Conflict of Interest

The authors have no conflicts to disclose.

Author Contributions

Anne C. Nickel: Formal analysis (lead); Investigation (lead); Writing - original draft (lead); Writing - review & editing (lead). Alan R. Denton: Formal analysis (supporting); Writing – original draft (supporting); Writing - review & editing (supporting). Judith E. Houston: Investigation (supporting); Writing - original draft (supporting); Writing - review & editing (supporting). Ralf Schweins: Investigation (supporting); Writing - original draft (supporting); Writing - review & editing (supporting). Tomàs S. Plivelic: Investigation (supporting); Writing - original draft (supporting); Writing - review & editing (supporting). Walter Richtering: Conceptualization (lead); Funding acquisition (lead); Supervision (supporting); Writing - original draft (supporting); Writing - review & editing (supporting). Andrea Scotti: Conceptualization (lead); Data curation (lead); Formal analysis (lead); Funding acquisition (lead); Investigation (lead); Supervision (lead); Writing - original draft (lead); Writing - review & editing (lead).

DATA AVAILABILITY

All the data used for this study are available at http://doi:10. 22000/692. SANS data are available at: http://doi.ill.fr/10.5291/ILL-DATA.9-10-1631.

APPENDIX A: CALCULATION OF NANOGEL DIMENSIONS WITHIN THE SANS MODEL

By fitting the SANS data with the ellipsoidal nanogel model,⁴⁴ the width of the hole (w_{core}), the width of the ith-shell (w_i), and the

fuzziness (σ) are obtained and can be used to probe how the nanogel architecture changes with increasing crowding. As hollow nanogels can differ in their fuzziness from the outer to the inner boundary, we distinguish between the internal fuzziness (σ_{in}) and the external (σ_{out}) fuzziness. For a two-shell model, we consider also an intermediate fuzziness (σ_{mid}). With these values, the short semi-axis (R_{SANS}) for a one-shell ellipsoid is calculated as follows:⁴⁴

$$R_{SANS} = w_{core} + 6\sigma_{in} + w_{core} + 6\sigma_{in} + w_{shell} + 6\sigma_{out}.$$
 (A1)

The long semi-axis $(L_{SANS}/2)$ can then be calculated with the aspect ratio (ε) ,

$$L_{SANS}/2 = \varepsilon R_{SANS}.$$
 (A2)

APPENDIX B: SYNTHESIS OF THE SACRIFICIAL ANISOTROPIC CORES

The procedure to obtain anisotropic nanogels in this work is adapted from the literature.⁴⁴ The different steps to synthesize the anisotropic cores^{89,90} are reported for the cores used for the hydrogenated anisotropic nanogels (HAN). The same hematite spindles were used for the deuterated anisotropic nanogels, and they were coated using a similar procedure to the one described in the following.

1. Hematite spindles

For the synthesis of hematite spindles, 85.5~g of $Fe(ClO_4)_3\cdot H_2O$, 10.27~g of urea, and 1.28~g of NaH_2PO_4 were dissolved in 1.7~l Milli-Q water inside a 2~l bottle and closed tightly with a cap. To ensure proper mixing, ultrasonication was used. The closed bottle was placed in an oven preheated to $98\,^{\circ}C$ for 24~h. Finally, the solution was centrifuged and redispersed in fresh Milli-Q water for purification and to obtain more highly concentrated samples.

2. PVP functionalization

A previous PVP stabilization is needed to achieve the silica coating of the hematite spindles. For this purpose, 17.2815 g of PVP was dissolved in 163 ml of Milli-Q water. This solution was filled in a three-neck flask, and an additional 100 ml of Milli-Q water was added. The three-neck flask was placed in an ultrasonic bath and equipped with an overhead stirrer. The ultrasonic bath was cooled with an external water cooling circle. After adding 4.7 ml of the hematite core solution in water (2.13 wt.%) to the flask, ultrasonication, stirring, and cooling were started. After 5 h, the ultrasonication was stopped. After another hour, the overhead stirrer was exchanged with a small stirring bar to stir the solution overnight. The solution was stirred for 24 h in total and afterward purified with three centrifugations of 90 min each with 5000 rpm. After the last centrifugation, the stabilized cores were redispersed in 25 ml of ethanol for the next synthesis step. For the synthesis of the deuterated anisotropic nanogels, 17.2815 g of PVP and 4.7 ml of hematite solution were used.

3. Silica shell

For the addition of the silica shell, a three-neck flask was filled with the 25 ml ethanol PVP functionalized hematite core solution. This flask was equipped with an overhead stirrer and placed inside

an ultrasonic bath. The ultrasonic bath was cooled by an external water cooling circle. After adding 186 ml of ethanol and 21 ml of doubled-distilled water to the three-neck flask, the stirrer and ultrasonication were started simultaneously. After 10 min, 88.7 µl of TMAH (25%) was added dropwise. Separately, 886 µl of TEOS and 612 μ l of ethanol were mixed and then divided into three parts of equal volumes. The three parts of the mixture were added to the three-neck flask dropwise after 35, 55, and 75 min of the addition of the TMAH. The ultrasonication was stopped after 3 h, and the overhead stirrer was exchanged with a normal stirring bar to stir the reaction solution overnight. After 24 h of stirring, the reaction solution was purified with three centrifugations and redispersion in fresh ethanol. After the last centrifugation, the ellipsoidal hematite-silica cores were redispersed in 17 ml of ethanol for the next synthesis step. For the synthesis of the deuterated anisotropic nanogels, 88.7 μ l of TMAH and 886 μ l of TEOS were used.

4. MPS functionalization

The hematite–silica cores in ethanol were sonicated for 15 min and then poured into a one-neck flask. Additional 11.8 ml of EtOH and 3.2 ml of NH $_3$ were added, and the solution was stirred with a magnetic stirring bar. 0.5 ml MPS were added dropwise, and the solution was stirred for 24 h. After 24 h, a reflux cooler was attached to the flask, and the solution was heated with an oil bath to 80 °C for 1 h. Afterward, the solution was centrifuged three times at room temperature for purification and redispersed in fresh ethanol. After the last centrifugation step, the functionalized hematite–silica core was redispersed in 3 ml of EtOH for the next synthesis step. For the synthesis of the deuterated anisotropic nanogels, 1.25 ml of MPS was used and the cores were redispersed in 5 ml EtOH.

5. Labeling of the samples

The HAN nanogels are identified as SFB985_A3_AN_M000653. The DAN nanogels are identified as SFB985_A3_AN_M000656. The DSN nanogels are identified as SFB985_A3_MB_M000234.

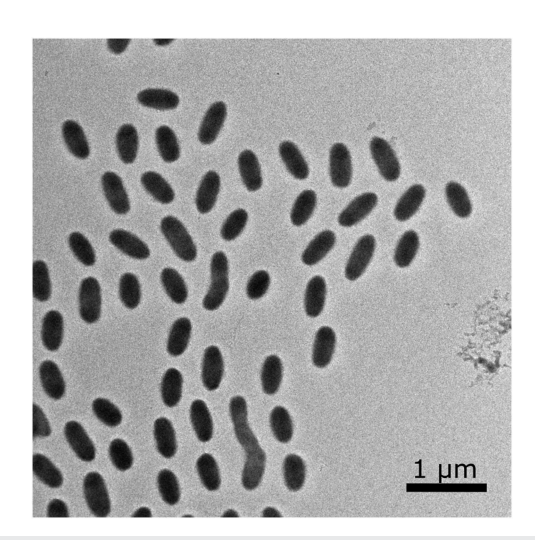


FIG. 7. Transmission electron microscopy image of the dried hydrogenated anisotropic nanogels after removal of the hematite–silica core.

APPENDIX C: TRANSMISSION ELECTRON MICROSCOPY (TEM)

Figure 7 shows a transmission electron microscopy image of the hydrogenated anisotropic nanogel (HAN) in the dry state. Elongated, homogeneously dark structures are visualized. This TEM image demonstrates the anisotropic shape of the nanogels and the successful etching of the hard core. Furthermore, the analysis of these images indicates that the size polydispersity of the nanogels is $\approx 15\%$, and a difference in the size polydispersity of the different axes is not appreciable within the experimental resolution.

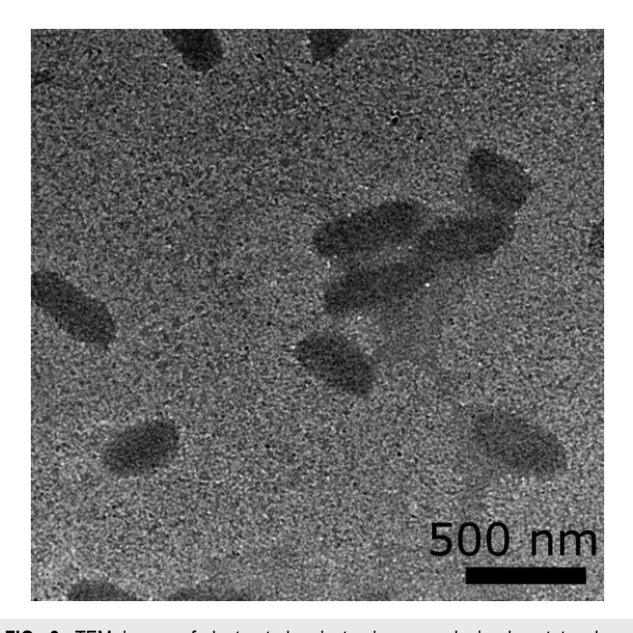


FIG. 8. TEM image of deuterated anisotropic nanogels in dry state shows anisotropically shaped nanogels.

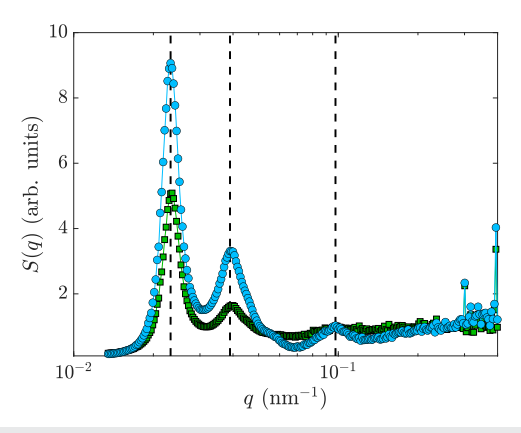
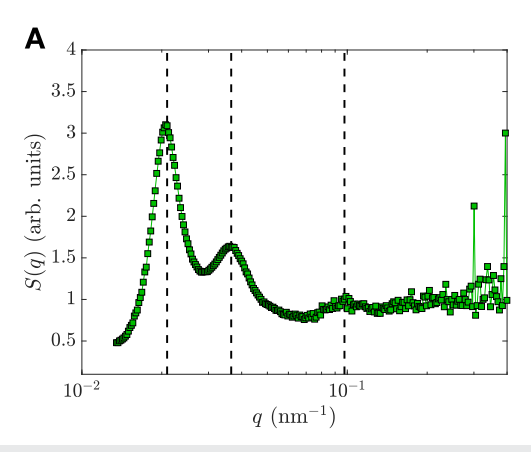


FIG. 9. Small-angle x-ray scattering structure factor of suspensions composed of only deuterated spherical nanogels (light blue circles) at $c_{DSN}=3.5$ wt. % and a mixture of the same deuterated spherical nanogels at $c_{DSN}=3.5$ wt. % mixed with protonated ellipsoidal nanogels (green squares) with a concentration of 0.4 wt. %. Dashed lines highlight the peak positions.



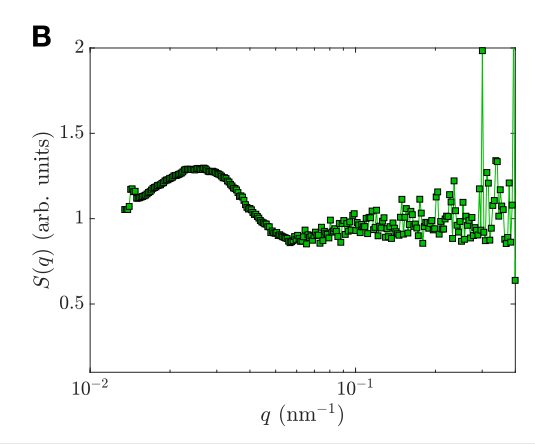


FIG. 10. Small-angle x-ray scattering structure factor of suspensions composed of a mixture of the deuterated spherical nanogels with protonated ellipsoidal nanogels. The concentration of the protonated ellipsoidal nanogels is constant and equal to 0.4 wt. %. The concentration of the spherical nanogels is $c_{DSN} = 2.4$ wt. % (a) and $c_{DSN} = 1.2$ wt. % (b). Dashed lines highlight the peak positions.

The TEM image was taken after drying the sample from a dispersion in water onto a TEM grid. Figure 7 indicates that solely the drying of the specimen without any compression leads to an ordering of the nanogels. Hence, the aspect ratio of HAN is large enough to induce an ordering based on the anisotropic shape of the nanogels.³⁴

Figure 8 shows a dry TEM image of DAN revealing an elongated shape and the etching of the hard core. This image makes clear that these deuterated nanogels provide a suitable matrix of nanogels for an anisotropic overcrowded environment.

APPENDIX D: SMALL-ANGLE X-RAY SCATTERING

Figures 9 and 10 show the structure factors S(q) = I(q) $/P_{DSN}(q)$, where I(q) is the measured intensity of a sample where few protonated anisotropic nanogels are embedded in a matrix of

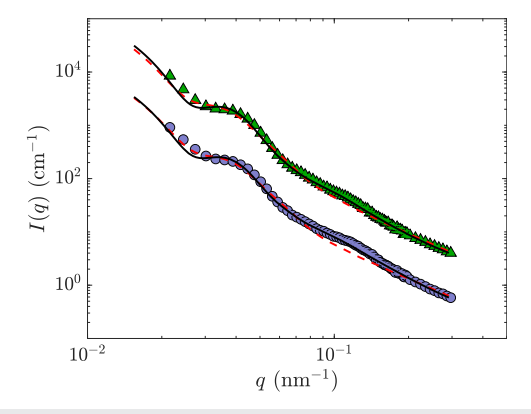


FIG. 11. Hydrogenated anisotropic nanogels mixed with two concentrations of deuterated anisotropic nanogels with their respective best fits with the one-shell (dashed red) and two-shell (solid black) ellipsoidal nanogel model. The circles correspond to the sample at $c=4.2\pm0.1$ wt. %, and the triangles correspond to the sample at $c=5.9\pm0.5$ wt. %.

deuterated spherical nanogels (DSN) and $P_{DSN}(q)$ is the form factor of the deuterated spherical nanogels measured under diluted conditions.

APPENDIX E: COMPARISON OF ONE-SHELL AND TWO-SHELL ELLIPSOID

Figure 11 shows the best fits obtained with the one-shell ellipsoidal nanogel model (dashed red lines) and the respective fits using the two-shell model (solid black lines) for HAN at two concentrations of DAN. The one-shell model is not appropriate to fit the intermediate *q*-region, making evident the need of a two-shell model. The necessity of a second shell in our model might indicate an inhomogeneous collapse of the polymeric network, resulting in a region of the nanogel with a considerably higher polymer fraction. In the future, computer simulations of realistic nanogels^{60,61,80} could be used to fully understand the microscopic meaning of a second shell to reproduce the SANS data.

REFERENCES

¹A. Scotti, M. F. Schulte, C. G. Lopez, J. J. Crassous, S. Bochenek, and W. Richtering, "How softness matters in soft nanogels and nanogel assemblies," Chem. Rev. **122**, 11675–11700 (2022).

²P. A. Janmey, J. P. Winer, and J. W. Weisel, "Fibrin gels and their clinical and bioengineering applications," J. R. Soc., Interface 6, 1–10 (2009).

³ A. C. Brown, S. E. Stabenfeldt, B. Ahn, R. T. Hannan, K. S. Dhada, E. S. Herman, V. Stefanelli, N. Guzzetta, A. Alexeev, W. A. Lam, L. A. Lyon, and T. H. Barker, "Ultrasoft microgels displaying emergent platelet-like behaviours," Nat. Mater. 13, 1108–1114 (2014).

⁴E. Tomasetti, R. Legras, B. Henri-Mazeaud, and B. Nysten, "Plastic deformation in polypropylene/(ethylene-propylene) copolymer blend during paint debonding," Polymer 41, 6597–6602 (2000).

⁵J. R. Stokes and W. J. Frith, "Rheology of gelling and yielding soft matter systems," Soft Matter 4, 1133–1140 (2008).

⁶D. Paloli, P. S. Mohanty, J. J. Crassous, E. Zaccarelli, and P. Schurtenberger, "Fluid-solid transitions in soft-repulsive colloids," Soft Matter **9**, 3000–3004 (2013).

- ⁷A. Scotti, U. Gasser, E. Herman, J. Han, A. Menzel, L. A. Lyon, and A. Fernandez-Nieves, "Phase behavior of binary and polydisperse suspensions of compressible microgels controlled by selective particle deswelling," Phys. Rev. E **96**, 032609 (2017).
- ⁸M. J. Bergman, N. Gnan, M. Obiols-Rabasa, J.-M. Meijer, L. Rovigatti, E. Zaccarelli, and P. Schurtenberger, "A new look at effective interactions between microgel particles," Nat. Commun. **9**, 5039 (2018).
- ⁹G. M. Conley, P. Aebischer, S. Nöjd, P. Schurtenberger, and F. Scheffold, "Jamming and overpacking fuzzy microgels: Deformation, interpenetration, and compression," Sci. Adv. 3, e1700969 (2017).
- ¹⁰H. Senff and W. Richtering, "Temperature sensitive microgel suspensions: Colloidal phase behavior and rheology of soft spheres," J. Chem. Phys. **111**, 1705–1711 (1999).
- ¹¹ A. Scotti, J. E. Houston, M. Brugnoni, M. Schmidt, M. Schulte, S. Bochenek, R. Schweins, A. Feoktystov, A. Radulescu, and W. Richtering, "Phase behavior of ultrasoft spheres show stable bcc lattices," Phys. Rev. E 102, 052602 (2020).
- ¹²M. Cloitre, R. Borrega, and L. Leibler, "Rheological aging and rejuvenation in microgel pastes," Phys. Rev. Lett. 85, 4819 (2000).
- ¹³C. Pellet and M. Cloitre, "The glass and jamming transitions of soft polyelectrolyte microgel suspensions," Soft Matter 12, 3710–3720 (2016).
- ¹⁴A. Scotti, M. Brugnoni, C. G. Lopez, S. Bochenek, J. J. Crassous, and W. Richtering, "Flow properties reveal the particle-to-polymer transition of ultra-low crosslinked microgels," Soft Matter 16, 668–678 (2020).
- ¹⁵ A. Ikeda, L. Berthier, and P. Sollich, "Unified study of glass and jamming rheology in soft particle systems," Phys. Rev. Lett. 109, 018301 (2012).
- ¹⁶S. Nandi, E. Mihalko, K. Nellenbach, M. Castaneda, J. Schneible, M. Harp, H. Deal, M. Daniele, S. Menegatti, T. H. Barker, and A. C. Brown, "Synthetic platelet microgels containing fibrin knob B mimetic motifs enhance clotting responses," Adv. Ther. 4, 2100010 (2021).
- ¹⁷J. Zhang, S. Yun, J. Bi, S. Dai, Y. Du, A. C. W. Zannettino, and H. Zhang, "Enhanced multi-lineage differentiation of human mesenchymal stem/stromal cells within poly(*N*-isopropylacrylamide-acrylic acid) microgel-formed three-dimensional constructs," J. Mater. Chem. B **6**, 1799–1814 (2018).
- ¹⁸ A. M. Douglas, A. A. Fragkopoulos, M. K. Gaines, L. A. Lyon, A. Fernandez-Nieves, and T. H. Barker, "Dynamic assembly of ultrasoft colloidal networks enables cell invasion within restrictive fibrillar polymers," Proc. Natl. Acad. Sci. U. S. A. 114, 885–890 (2017).
- ¹⁹ A. Scotti, S. Bochenek, M. Brugnoni, M.-A. Fernandez-Rodriguez, M. F. Schulte, J. E. Houston, A. P. Gelissen, I. I. Potemkin, L. Isa, and W. Richtering, "Exploring the colloid-to-polymer transition for ultra-low crosslinked microgels from three to two dimensions," Nat. Commun. 10, 1418 (2019).
- ²⁰ M. Karg, A. Pich, T. Hellweg, T. Hoare, L. A. Lyon, J. J. Crassous, D. Suzuki, R. A. Gumerov, S. Schneider, I. I. Potemkin, and W. Richtering, "Nanogels and microgels: From model colloids to applications, recent developments, and future trends," Langmuir 35, 6231–6255 (2019).
- ²¹G. M. Conley, C. Zhang, P. Aebischer, J. L. Harden, and F. Scheffold, "Relationship between rheology and structure of interpenetrating, deforming and compressing microgels," Nat. Commun. 10, 2436–2438 (2019).
- ²² M. Stieger, P. Lindner, and W. Richtering, "Structure formation in thermore-sponsive microgel suspensions under shear flow," J. Phys.: Condens. Matter 16, S3861 (2004).
- ²³ M. R. Islam, R. Nguyen, and L. A. Lyon, "Emergence of non-hexagonal crystal packing of deswollen and deformed ultra-soft microgels under osmotic pressure control," <u>Macromol. Rapid Commun.</u> 42, 2100372 (2021).
- ²⁴T. Höfken, C. Strauch, S. Schneider, and A. Scotti, "Changes in the form factor and size distribution of nanogels in crowded environments," Nano Lett. 22, 2412–2418 (2022).
- ²⁵ A. S. J. Iyer and L. A. Lyon, "Self-healing colloidal crystals," Angew. Chem. 121, 4632–4636 (2009).
- ²⁶D. Frenkel, "Soft particles feel the squeeze," Nature 460, 465–466 (2009).
- ²⁷ A. Scotti, U. Gasser, E. S. Herman, M. Pelaez-Fernandez, J. Han, A. Menzel, L. A. Lyon, and A. Fernández-Nieves, "The role of ions in the self-healing behavior of soft particle suspensions," Proc. Natl. Acad. Sci. U. S. A. 113, 5576–5581 (2016).
 ²⁸ U. Gasser, A. Scotti, and A. Fernandez-Nieves, "Spontaneous deswelling of

microgels controlled by counterion clouds," Phys. Rev. E 99, 042602 (2019).

- ²⁹J. J. Crassous, A. M. Mihut, E. Wernersson, P. Pfleiderer, J. Vermant, P. Linse, and P. Schurtenberger, "Field-induced assembly of colloidal ellipsoids into well-defined microtubules," Nat. Commun. 5, 5516 (2014).
- ³⁰ A. Pal, V. A. Martinez, T. H. Ito, J. Arlt, J. J. Crassous, W. C. Poon, and P. Schurtenberger, "Anisotropic dynamics and kinetic arrest of dense colloidal ellipsoids in the presence of an external field studied by differential dynamic microscopy," Sci. Adv. 6, eaaw9733 (2020).
- ³¹ A. Donev, F. H. Stillinger, P. M. Chaikin, and S. Torquato, "Unusually dense crystal packings of ellipsoids," Phys. Rev. Lett. **92**, 255506 (2004).
- ³²A. Doney, I. Cisse, D. Sachs, E. A. Variano, F. H. Stillinger, R. Connelly,
 S. Torquato, and P. M. Chaikin, "Improving the density of jammed disordered packings using ellipsoids," Science 303, 990–993 (2004).
 ³³D. Parisi, Y. Ruan, G. Ochbaum, K. S. Silmore, L. L. Cullari, C.-Y. Liu, R. Bitton,
- ³³D. Parisi, Y. Ruan, G. Ochbaum, K. S. Silmore, L. L. Cullari, C.-Y. Liu, R. Bitton, O. Regev, J. W. Swan, B. Loppinet, and D. Vlassopoulos, "Short and soft: Multidomain organization, tunable dynamics, and jamming in suspensions of grafted colloidal cylinders with a small aspect ratio," Langmuir 35, 17103–17113 (2019).
- ³⁴A. C. Nickel, T. Kratzenberg, S. Bochenek, M. M. Schmidt, A. A. Rudov, A. Falkenstein, I. I. Potemkin, J. J. Crassous, and W. Richtering, "Anisotropic microgels show their soft side," Langmuir 38, 5063–5080 (2021).
- ³⁵S. E. A. Gratton, P. A. Ropp, P. D. Pohlhaus, J. C. Luft, V. J. Madden, M. E. Napier, and J. M. DeSimone, "The effect of particle design on cellular internalization pathways," Proc. Natl. Acad. Sci. U. S. A. 105, 11613–11618 (2008).
- ³⁶L. Florez, C. Herrmann, J. M. Cramer, C. P. Hauser, K. Koynov, K. Landfester, D. Crespy, and V. Mailänder, "How shape influences uptake: Interactions of anisotropic polymer nanoparticles and human mesenchymal stem cells," Small 8, 2222–2230 (2012).
- ³⁷O. Shimoni, Y. Yan, Y. Wang, and F. Caruso, "Shape-dependent cellular processing of polyelectrolyte capsules," ACS Nano 7, 522–530 (2013).
- ³⁸S. Dasgupta, T. Auth, and G. Gompper, "Shape and orientation matter for the cellular uptake of nonspherical particles," Nano Lett. **14**, 687–693 (2014).
- ³⁹ X. Chen, Y. Yan, M. Müllner, Y. Ping, J. Cui, K. Kempe, C. Cortez-Jugo, and F. Caruso, "Shape-dependent activation of cytokine secretion by polymer capsules in human monocyte-derived macrophages," Biomacromolecules 17, 1205–1212 (2016).
- ⁴⁰B. Xue, V. Kozlovskaya, and E. Kharlampieva, "Shaped stimuli-responsive hydrogel particles: Syntheses, properties and biological responses," J. Mater. Chem. B 5, 9–35 (2017).
- ⁴¹A. Pepe, P. Podesva, and G. Simone, "Tunable uptake/release mechanism of protein microgel particles in biomimicking environment," Sci. Rep. 7, 6014–6018 (2017).
- ⁴²J. C. Rose, M. Cámara-Torres, K. Rahimi, J. Köhler, M. Möller, and L. De Laporte, "Nerve cells decide to orient inside an injectable hydrogel with minimal structural guidance," Nano Lett. 17, 3782–3791 (2017).
- ⁴³J. C. Rose, D. B. Gehlen, T. Haraszti, J. Köhler, C. J. Licht, and L. De Laporte, "Biofunctionalized aligned microgels provide 3D cell guidance to mimic complex tissue matrices," Biomaterials 163, 128–141 (2018).
- ⁴⁴A. C. Nickel, A. Scotti, J. E. Houston, T. Ito, J. Crassous, J. S. Pedersen, and W. Richtering, "Anisotropic hollow microgels that can adapt their size, shape, and softness," Nano Lett. **19**, 8161–8170 (2019).
- ⁴⁵K. Honda, Y. Sazuka, K. Iizuka, S. Matsui, T. Uchihashi, T. Kureha, M. Shibayama, T. Watanabe, and D. Suzuki, "Hydrogel microellipsoids that form robust string-like assemblies at the air/water interface," Angew. Chem., Int. Ed. 58, 7294–7298 (2019).
- ⁴⁶A. Scotti, M. Brugnoni, A. A. Rudov, J. E. Houston, I. I. Potemkin, and W. Richtering, "Hollow microgels squeezed in overcrowded environments," J. Chem. Phys. 148, 174903 (2018).
- ⁴⁷A. Scotti, A. Denton, M. Brugnoni, R. Schweins, and W. Richtering, "Absence of crystals in the phase behavior of hollow microgels," Phys. Rev. E **103**, 022612 (2021).
- ⁴⁸ A. Scotti, "Characterization of the volume fraction of soft deformable microgels by means of small-angle neutron scattering with contrast variation," Soft Matter 17, 5548–5559 (2021).
- ⁴⁹T. S. Plivelic, A. E. Terry, R. Appio, K. Theodor, and K. Klementiev, "X-ray tracing, design and construction of an optimized optics scheme for CoSAXS, the small angle x-ray scattering beamline at MAX IV laboratory," AIP Conf. Proc. **2054**, 030013 (2019).

- ⁵⁰J. Filik, A. W. Ashton, P. C. Y. Chang, P. A. Chater, S. J. Day, M. Drakopoulos, M. W. Gerring, M. L. Hart, O. V. Magdysyuk, S. Michalik *et al.*, "Processing two-dimensional X-ray diffraction and small-angle scattering data in *DAWN 2*," J. Appl. Crystallogr. **50**, 959–966 (2017).
- ⁵¹ M. Urich and A. R. Denton, "Swelling, structure, and phase stability of compressible microgels," Soft Matter 12, 9086–9094 (2016).
- ⁵²T. J. Weyer and A. R. Denton, "Concentration-dependent swelling and structure of ionic microgels: Simulation and theory of a coarse-grained model," Soft Matter 14, 4530–4540 (2018).
- ⁵³ P. J. Flory, *Principles of Polymer Chemistry* (Cornell University Press, Ithaca, 1953).
- ⁵⁴P. J. Flory and J. Rehner, "Statistical mechanics of cross-linked polymer networks I. Rubberlike elasticity," J. Chem. Phys. 11, 512–520 (1943).
- ⁵⁵P. J. Flory and J. Rehner, "Statistical mechanics of cross-linked polymer networks II. Swelling," J. Chem. Phys. **11**, 521–526 (1943).
- ⁵⁶L. D. Landau and E. M. Lifshitz, *Theory of Elasticity*, 3rd ed. (Elsevier, Amsterdam, 1986).
- ⁵⁷C. G. Lopez and W. Richtering, "Does Flory-Rehner theory quantitatively describe the swelling of thermoresponsive microgels?," Soft Matter 13, 8271–8280 (2017).
- ⁵⁸P.-G. de Gennes, Scaling Concepts in Polymer Physics (Cornell, Ithaca, 1979).
- ⁵⁹ A. Scotti, A. R. Denton, M. Brugnoni, J. E. Houston, R. Schweins, I. I. Potemkin, and W. Richtering, "Deswelling of microgels in crowded suspensions depends on cross-link density and architecture," <u>Macromolecules</u> 52, 3995–4007 (2019).
- ⁶⁰N. Gnan, L. Rovigatti, M. Bergman, and E. Zaccarelli, "In silico synthesis of microgel particles," Macromolecules 50, 8777–8786 (2017).
- ⁶¹ L. Rovigatti, N. Gnan, A. Ninarello, and E. Zaccarelli, "Connecting elasticity and effective interactions of neutral microgels: The validity of the Hertzian model," Macromolecules 52, 4895–4906 (2019).
- $^{\bf 62}$ H. Gould, J. Tobochnik, and W. Christian, Introduction to Computer Simulation Methods (Addison-Wesley, 2006).
- ⁶³D. Frenkel and B. Smit, *Understanding Molecular Simulation*, 2nd ed. (Academic, London, 2001).
- ⁶⁴K. Binder and D. W. Heermann, Monte Carlo Simulation in Statistical Physics: An Introduction, 5th ed. (Springer, Berlin, 2010).
- $^{65}\rm W.$ K. Lim and A. R. Denton, "Polymer crowding and shape distributions in polymer-nanoparticle mixtures," J. Chem. Phys. 141, 114909 (2014).
- ⁶⁶W. K. Lim and A. R. Denton, "Depletion-induced forces and crowding in polymer-nanoparticle mixtures: Role of polymer shape fluctuations and penetrability," J. Chem. Phys. 144, 024904 (2016).
- ⁶⁷W. K. Lim and A. R. Denton, "Influence of polymer shape on depletion potentials and crowding in colloid-polymer mixtures," Soft Matter 12, 2247-2252 (2016).
- ⁶⁸ W. J. Davis and A. R. Denton, "Influence of solvent quality on conformations of crowded polymers," J. Chem. Phys. **149**, 124901 (2018).
- ⁶⁹A. R. Denton and W. J. Davis, "Influence of solvent quality on depletion potentials in colloid-polymer mixtures." J. Chem. Phys. 155, 084904 (2021).
- potentials in colloid–polymer mixtures," J. Chem. Phys. 155, 084904 (2021). ⁷⁰J. C. Hart, "Distance to an ellipsoid," in *Graphics Gems IV*, edited by P. S. Heckbert (Academic, San Diego, 1994), pp. 113–119.
- ⁷¹ U. Gasser, J. S. Hyatt, J.-J. Lietor-Santos, E. S. Herman, L. A. Lyon, and A. Fernandez-Nieves, "Form factor of pNIPAM microgels in overpacked states," J. Chem. Phys. 141, 034901 (2014).

- ⁷² P. S. Mohanty, S. Nöjd, K. van Gruijthuijsen, J. J. Crassous, M. Obiols-Rabasa, R. Schweins, A. Stradner, and P. Schurtenberger, "Interpenetration of polymeric microgels at ultrahigh densities," Sci. Rep. 7, 1487 (2017).
- ⁷³ S. Nöjd, P. Holmqvist, N. Boon, M. Obiols-Rabasa, P. S. Mohanty, R. Schweins, and P. Schurtenberger, "Deswelling behaviour of ionic microgel particles from low to ultra-high densities," Soft Matter 14, 4150–4159 (2018).
- ⁷⁴ A. Scotti, U. Gasser, A. V. Petrunin, L. Fruhner, W. Richtering, and J. E. Houston, "Experimental determination of the bulk moduli of hollow nanogels," Soft Matter 18, 5750–5758 (2022).
- 75 F. S. Varley, "Neutron scattering lengths and cross section," Neutron News 3, 29–37 (1992).
- ⁷⁶G. K. Batchelor, "The effect of Brownian motion on the bulk stress in a suspension of spherical particles," J. Fluid Mech. **83**, 97–117 (1977).
- ⁷⁷G. Brambilla, D. El Masri, M. Pierno, L. Berthier, L. Cipelletti, G. Petekidis, and A. B. Schofield, "Probing the equilibrium dynamics of colloidal hard spheres above the mode-coupling glass transition," Phys. Rev. Lett. 102, 085703 (2009).
- ⁷⁸P. Van Der Scheer, T. Van De Laar, J. Van Der Gucht, D. Vlassopoulos, and J. Sprakel, "Fragility and strength in nanoparticle glasses," ACS Nano 11, 6755–6763 (2017).
- ⁷⁹M. Pelaez-Fernandez, A. Souslov, L. Lyon, P. M. Goldbart, and A. Fernandez-Nieves, "Impact of single-particle compressibility on the fluid-solid phase transition for ionic microgel suspensions," Phys. Rev. Lett. 114, 098303 (2015).
- ⁸⁰S. V. Nikolov, A. Fernandez-Nieves, and A. Alexeev, "Behavior and mechanics of dense microgel suspensions," Proc. Natl. Acad. Sci. U. S. A. 117, 27096–27103 (2020)
- ⁸¹F. Scheffold and T. G. Mason, "Scattering from highly packed disordered colloids," J. Phys.: Condens. Matter 21, 332102 (2009).
- ⁸²M. Breitenstein, U. Kräuter, and U. Riebel, "The fundamentals of particle size analysis by transmission fluctuation spectrometry. Part 1: A theory of temporal transmission fluctuations in dilute suspensions," Part. Part. Syst. Charact. 16, 249–256 (1999).
- 83 J. E. Houston, L. Fruhner, A. de la Cotte, J. Rojo González, A. V. Petrunin, U. Gasser, R. Schweins, J. Allgaier, W. Richtering, A. Fernandez-Nieves, and A. Scotti, "Resolving the different bulk moduli within individual soft nanogels using small-angle neutron scattering," Sci. Adv. 8, eabn6129 (2022).
- ⁸⁴I. Bouhid de Aguiar, T. van de Laar, M. Meireles, A. Bouchoux, J. Sprakel, and K. Schroën, "Deswelling and deformation of microgels in concentrated packings," Sci. Rep. 7, 10223 (2017).
- ⁸⁵Z. Zhang, N. Krishna, M. P. Lettinga, J. Vermant, and E. Grelet, "Reversible gelation of rod-like viruses grafted with thermoresponsive polymers," Langmuir 25, 2437–2442 (2009).
- ⁸⁶M. J. Solomon and P. T. Spicer, "Microstructural regimes of colloidal rod suspensions, gels, and glasses," Soft Matter 6, 1391–1400 (2010).
- 87 A. Scotti, M. Pelaez-Fernandez, U. Gasser, and A. Fernandez-Nieves, "Osmotic pressure of suspensions comprised of charged microgels," Phys. Rev. E 103, 012609 (2021).
- ⁸⁸P. M. Chaikin, A. Donev, W. Man, F. H. Stillinger, and S. Torquato, "Some observations on the random packing of hard ellipsoids," Ind. Eng. Chem. Res. **45**, 6960–6965 (2006).
- 89 M. Ocaña, M. P. Morales, and C. J. Serna, "Homogeneous precipitation of uniform α -Fe₂O₃ particles from iron salts solutions in the presence of urea," J. Colloid Interface Sci. **212**, 317–323 (1999).
- ⁹⁰C. Graf, D. L. J. Vossen, A. Imhof, and A. van Blaaderen, "A general method to coat colloidal particles with silica," Langmuir 19, 6693–6700 (2003).